Nanoscale control of single molecule Förster resonance energy transfer by a scanning photonic nanoantenna

Maria Sanz-Paz, Jérôme Wenger, Niek F van Hulst, Mathieu Mivelle, Maria F Garcia-Parajo

Research article

Maria Sanz-Paz, Jerome Wenger, Niek F. van Hulst, Mathieu Mivelle* and Maria F. Garcia-Parajo*

Nanoscale control of single molecule Förster resonance energy transfer by a scanning photonic nanoantenna

https://doi.org/10.1515/nanoph-2020-0221
Received March 31, 2020; accepted May 30, 2020

Abstract: Förster Resonance Energy Transfer (FRET) is a widely applied technique in biology to accurately measure intra- and inter-molecular interactions at the nanometre scale. FRET is based on near-field energy transfer from an excited donor to a ground state acceptor emitter. Photonic nanoantennas have been shown to modify the rate, efficiency and extent of FRET, a process that is highly dependent on the near-field gradient of the antenna field as felt by the emitters, and thus, on their relative distance. However, most of the experiments reported to date focus on fixed antennas where the emitters are either immobilized or diffusing in solution, so that the distance between the antenna and the emitters cannot be manipulated. Here, we use scanning photonic nanoantenna probes to directly modulate the FRET efficiency between individual FRET pairs with an unprecedented nanometric lateral precision of 2 nm on the antenna position. We find that the antenna acts as an independent acceptor element, competing with the FRET pair acceptor. We directly map the competition between FRET and donor-antenna transfer as a function of the relative position between the antenna and the FRET donor-acceptor pair. The experimental data are well-described by FDTD simulations, confirming that the modulation of FRET efficiency is due to the spatially dependent coupling of the single FRET pair to the photonic antenna.

Keywords: fluorescence enhancement; FRET; near-field fluorescence microscopy; photonic nanoantennas; plasmonic antennas.

1 Introduction

Metallic nanostructures, also called photonic nanoantennas, can convert propagating electromagnetic waves into localized fields at the nanometre scale, and vice versa [1]. Through plasmonic resonances, metallic nanoantennas enhance and confine electromagnetic fields much below the wavelength of light. This property has been used for many purposes, ranging from super-resolution microscopy [2] or biosensing at high concentrations [3] to detection of dynamic events at the nanometre scale [4], and, in particular, to enhance the fluorescence of single emitters placed in their vicinity by manipulating both excitation and emission processes [1, 5]. Indeed, photonic antennas modify the local density of states (LDOS) in their vicinity, which in turn affects the total ($k_{tot} = k_r + k_{nr}$), radiative (k_r) and non radiative (k_{nr}) decay rates of nearby quantum emitters [6]. This has the effect of reducing the fluorescence lifetime τ of the emitters ($\tau = (k_r + k_{nr})^{-1}$), and modifying their quantum yield ϕ ($\phi = k_r/(k_r + k_{nr})$). Interestingly, the latter can either be decreased or increased by the presence of the antenna, depending on the intrinsic quantum yield of the emitter and the competition between k_r and k_{nr} that the antenna generates [7]. Moreover, the fluorescence intensity I emitted by a single emitter is given by $I = k_{exc} \cdot \phi$, where k_{exc} is the excitation rate given by the incident field. Thus, the emitted fluorescence can be also enhanced by the photonic antenna, if the quantum yield and/or the excitation field are increased by the nanostructure [8].

***Corresponding authors: Maria F. Garcia-Parajo**, ICFO-Institut de Ciencies Fotoniques, The Barcelona Institute for Science and Technology, 08860, Barcelona, Spain; and ICREA, Pg. Lluis Companys 23, 08010, Barcelona, Spain, E-mail: maria.garcia-parajo@icfo.eu; and **Mathieu Mivelle**, Sorbonne Université, CNRS, Institut des NanoSciences de Paris, UMR 7588, 75005, Paris, France, E-mail: mathieu.mivelle@sorbonne-universite.fr. https://orcid.org/0000-0001-6618-3944 (M.-F. Garciarajo)
Maria Sanz-Paz: ICFO-Institut de Ciencies Fotoniques, The Barcelona Institute for Science and Technology, 08860, Barcelona, Spain
Jerome Wenger: Aix Marseille Univ, CNRS, Centrale Marseille, Institut Fresnel, 13013, Marseille, France
Niek F. van Hulst: ICFO-Institut de Ciencies Fotoniques, The Barcelona Institute for Science and Technology, 08860, Barcelona, Spain; ICREA, Pg. Lluis Companys 23, 08010, Barcelona, Spain

Over the past decade, all of these properties have triggered the application of photonic antennas towards the manipulation of single molecule fluorescence emission demonstrating detection of single molecules at ultra-high concentrations [3, 9], fluorescence enhancement [10] or super-resolution imaging [11, 12]. More recently, it has been discovered that nanoantennas can influence, and even improve, the efficiency of Förster Resonance Energy Transfer (FRET) [13–15]. FRET is based on the near-field energy transfer between two emitters, from an excited donor to a ground state acceptor. The FRET efficiency, E_{FRET} i.e. the probability that the acceptor will receive the energy once the donor is excited is given by [16]:

$$E_{FRET} = \frac{k_{FRET}}{k_{FRET} + k_d} = \frac{1}{1 + \left(\frac{R}{R_0}\right)^6} \quad (1)$$

where k_{FRET} corresponds to the FRET decay rate, and k_d is the donor decay emission rate (where $k_d = \frac{1}{\tau_d}$; τ_d being the donor lifetime [16]). R is the distance between donor and acceptor, and R_0 is the so-called Förster radius, i.e. the distance at which E_{FRET} is 50%. R_0 depends on the overlap integral of the donor emission with the absorption spectrum of the acceptor and their mutual dipolar orientation κ. Due to the strong distance dependence between donor and acceptor, FRET is used to accurately measure the nanometric distance between two fluorescent emitters (typically in the range of 1–10 nm) and it is widely applied in biology and chemistry [13, 17].

From the excitation point of view, photonic antennas can open new energy transfer routes due to the strong confinement of the near-field becoming comparable to the donor-acceptor distance [18], whereas the modification of the LDOS can affect both, the k_{FRET} and the decay rates of both donor and acceptor [19, 20]. As a result, the two main parameters used to experimentally characterize FRET: k_{FRET} and E_{FRET} can be modified by the presence of the antenna [21–24].

Recent studies on the effect of nanoantennas on the process of FRET show that they can help overcoming some of the main limitations of conventional FRET: they can extend the range at which energy transfer occurs [25–27] and they can mediate the transfer between perpendicularly oriented dipoles [18, 28]. Such advantages make plasmon-assisted FRET a promising strategy for molecular biology. One of the already demonstrated applications uses FRET combined with silver nanoparticles to detect protein-specific sialylation on the cell surface by taking advantage of the enhancement of both the FRET fluorescence signal (having thus a higher contrast) and the FRET efficiency [29]. A second application monitors conformational changes of proteins in living cells with higher sensitivity than with conventional methods thanks to the increased sensitivity to detect changes in FRET efficiency provided by gold-coated coverslips [28].

An additional effect of the coupling between photonic antennas and emitters is the modification of the spatial emission and directionality of the fluorescence emission [30–33]. When in resonance, the emitter couples to the nanoantenna so that the radiation proceeds from the coupled system, giving rise to changes in the angular emission. Such changes in emission directionality can be tuned by shifting the antenna resonance and/or by modifying the orientation or the position of the emitter with respect to the antenna. This spatial redistribution of the emission also has an impact on FRET as k_{FRET} is proportional to the field emitted by the donor at the acceptor position [34]. Thus, the FRET rate enhancement can be calculated by computing the ratio between the donor emission in presence and absence of the antenna. By performing such calculations for different acceptor positions, a spatial mapping of the FRET rate enhancement can be readily obtained. Using Finite Difference Time Domain (FDTD) simulations to calculate the donor emission, it has been shown that such enhancement is a function of both the position [19] and the orientation [26] of the donor within the antenna field. However, experiments aimed to validate these simulations have been performed on diffusing emitters, where there is no control over the position or orientation of the emitters with respect to the antenna. This drawback can be partially overcome by making use of DNA origamis to immobilize the FRET pair at designed positions with respect to the antenna [20, 33, 35]. Yet, such approach is static, and only one relative position can be probed on a specific origami construct.

Here, we demonstrate the use of photonic nanoantennas fabricated at the apex of near-field scanning optical microscopy (NSOM) probes to accurately control the 3D position of antennas over individual FRET pairs, with 2 nm lateral precision. We experimentally demonstrate modulation of the FRET efficiency up to 15%, at the level of a single FRET pair. Such modulation depends on the relative distance between the antenna and the FRET donor and acceptor pair, and on the donor dipole orientation. Our experimental results, supported by FDTD simulations, directly reveal the competition between FRET donor-acceptor transfer and the donor-antenna transfer, while scanning and controlling the donor-antenna distance on the nanometre scale.

2 Results and discussion

Figure 1A describes the principle of the experiments described here, where a photonic nanoantenna laterally scans individual FRET pairs with nanometric precision. By varying the relative position between the antenna and the pair during scanning, one obtains a super-resolution map of the antenna-to-FRET-pair coupling, and its impact on k_d, k_{FRET} and resulting FRET efficiency. The experiments have been performed using a homemade combined confocal/NSOM setup (Figure 1B). Excitation of the sample is achieved either in confocal mode (not shown in the figure), or by coupling the laser light ($\lambda = 561$ nm, 100 nW) at the backend of a near-field probe supporting a monopole on a bowtie antenna at its apex. Experiments in confocal mode are performed using circularly polarized light, while excitation via the antenna is performed by adjusting the incoming polarized light along the bowtie gap region to drive the gap mode. The sample is mounted on a piezo stage that can be scanned in 3D with nanometre accuracy. The fluorescence emitted from the sample is collected through a 1.3 NA objective and split towards two single-photon counting avalanche photodiodes (SPADs) to discriminate the light emitted from the acceptor and donor molecules.

The antenna geometry used in our experiments is a "hybrid" antenna that consists on a bowtie nanoantenna resonator (BNA) that couples the light onto a monopole [11] (Figure 1B, inset). The antennas are fabricated at the apex of aluminium coated tapered optical fibres using focussed ion beam (FIB) and mounted on the NSOM head (Figure 1B). The FRET sample consists of double-stranded DNA molecules of 51 base pairs total length, labelled with a single Atto550 donor and a single Atto647N as acceptor, set at specific positions on the DNA double strand to reach a separation of 10 base pairs. In these conditions, the donor–acceptor distance is estimated to be around 3.4 nm, which is about twice lower than the Förster radius of $R_0 = 6.5$ nm, assuming an average orientational factor $\kappa^2 = 2/3$ for this set of fluorescent dyes. The FRET pairs are spin coated and immobilized on PMMA-coated coverslips (10 nm layer) at low concentrations to allow for single-pair FRET measurements both in confocal and NSOM modes. A second thin PMMA layer (~ 10 nm) is spin-coated on top of the FRET pairs to prevent possible dragging by the antenna and to improve the photophysical stability of the dyes (Figure 1B, inset). Considering that the axial separation between the antenna probe and the PMMA surface as maintained by the NSOM feedback loop is between 5 and 10 nm (± 1 nm) [2, 11], the actual axial distance between the FRET pairs and the antenna is between 15 and 20 nm.

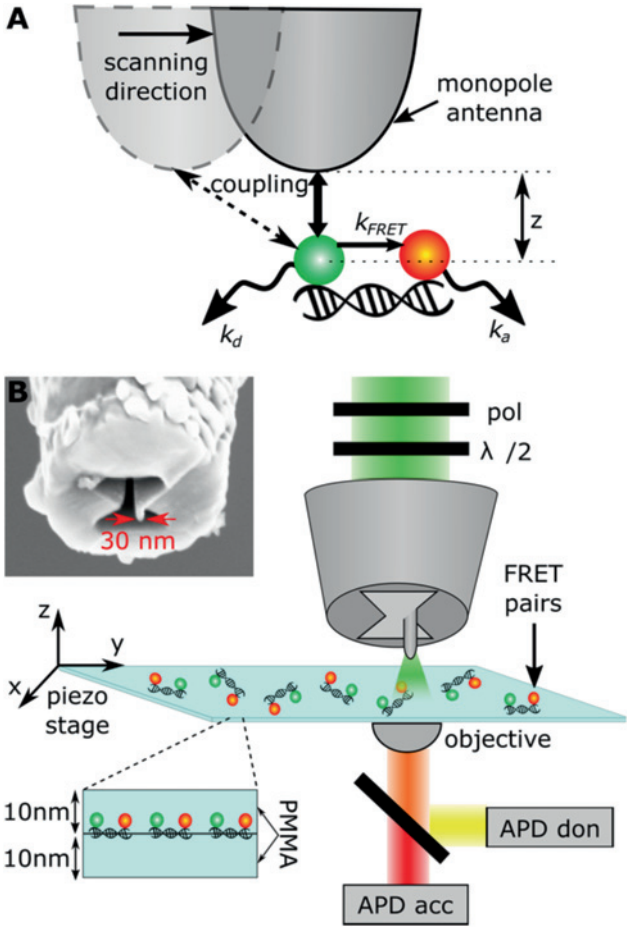

Figure 1: (A) Schematic depiction of the Förster resonance energy transfer (FRET) process in presence of a scanning antenna, showing the different rates involved. An optical nanoantenna (bowtie with monopole) positioned at a z distance above the sample scans laterally individual FRET pairs. The coupling of the monopole antenna to the emitters depends on their relative 3D position and affects the donor decay rate k_d and k_{FRET}, modulating FRET efficiency and acceptor emission. (B) Schematic of the near-field scanning optical microscopy (NSOM) setup, with an aluminium-based optical antenna probe placed in close proximity to the sample, where the FRET pairs are immobilized, and the subsequent detection scheme. The upper inset shows a scanning electron microscope (SEM) image of a representative hybrid antenna probe supporting a monopole with an apex of 30 nm in diameter. The lower inset shows a cross-section of the sample, with the FRET pairs immobilized between two 10 nm think-poly (methyl methacrylate (PMMA) layers.

According to FDTD simulations our hybrid antenna design provides an intensity enhancement of up to 500-fold (Figure 2A) for an incident polarization along the gap and a spatial confinement (30–50 nm) that matches the diameter of the monopole [11]. Due to its geometry, the near-field intensities close to the monopole end exhibit

different patterns and degree of enhancement for all 3D orientations (Figure 2A), which in turn will affect how dipoles with different orientations are excited. Importantly, the selected design and metal used make these types of antennas broadband over the visible range of the spectrum (Figure 2B) significantly overlapping with the absorption and emission spectra of both donor and acceptor dyes used in our experiments (Figure 2B).

A representative confocal image of individual FRET pairs is shown in Figure 3A. Each spot on the image corresponds to the fluorescence emission of a *single* FRET pair, where magenta and green represent the acceptor and donor channels respectively. As expected, most of the spots are magenta, consistent with the short distances involved and the estimated $E_{FRET} \sim 98\%$. We attribute the few green spots observed mostly to the fact that the DNA hybridization is not 100% efficient and a non-negligible probability that the two emitters are perpendicular to each other, so that FRET does not occur. Figure 3B, C shows two exemplary near-field images obtained on smaller regions of the sample using a hybrid nanoantenna. Similar to the confocal case, most of the fluorescence spots are magenta, indicative of high FRET efficiency. In addition, the fluorescence spots show characteristic near-field patterns, i.e. a central bright spot having a full-width-at-half-maximum (FWHM) around 50 nm corresponding to the highly confined excitation from the monopole, together with a weaker shadow region on a side, resulting from residual excitation of the BNA arms. Moreover, based on the FDTD simulations and excitation patterns shown in Figure 2, the near-field spots obtained in these

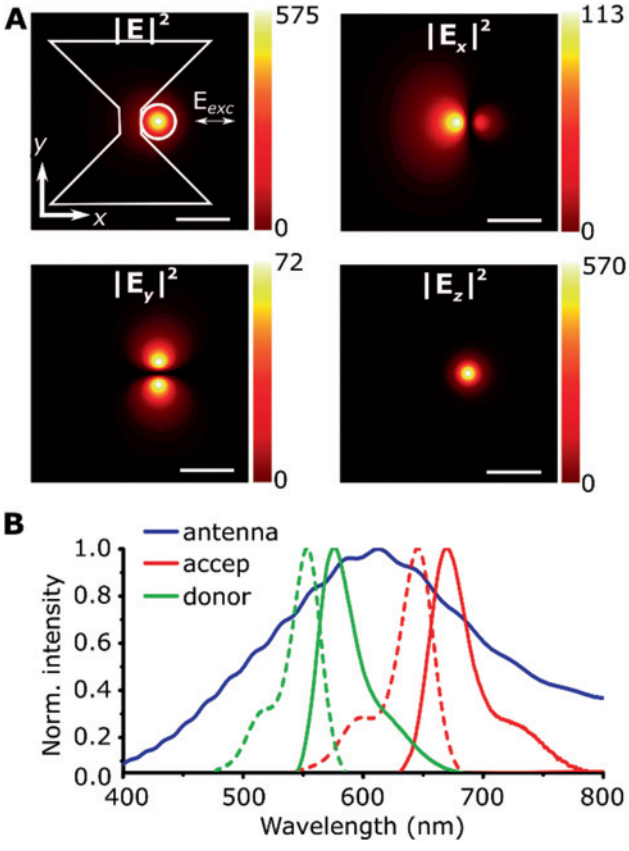

Figure 2: (A) FDTD simulations of the near-field intensity enhancement (ratio of intensity in presence and absence of the antenna) provided by a hybrid antenna (30 nm in diameter, 70 nm in length), 10 nm away from the monopole end. Both the total field as well as the *x*, *y*, and *z* components of the near-field are displayed. Scale bars: 100 nm. (B) Absorption (dashed lines) and emission (solid lines) spectra of both the donor (green) and acceptor (red) dyes. The broad resonance spectrum of the hybrid antenna obtained from FDTD simulations is shown in blue.

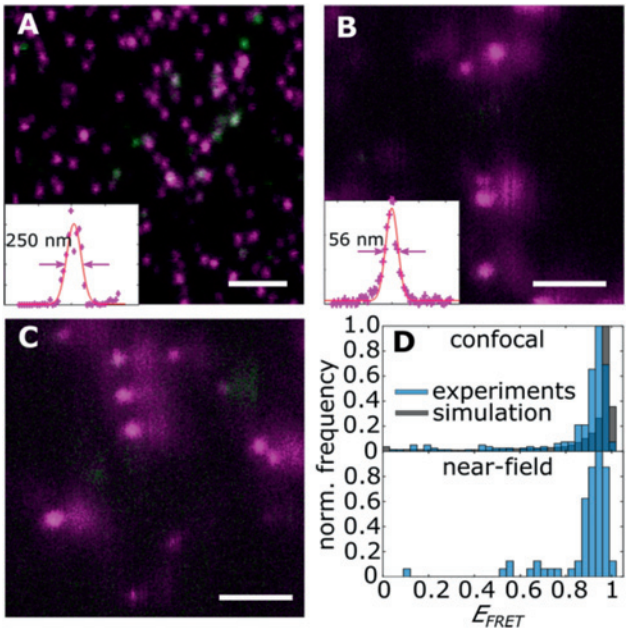

Figure 3: (A) Representative confocal image of a sample containing individual 3.4 nm FRET pairs. Magenta represents signal from the acceptor channel (178 counts/ms) and green from the donor channel (55 counts/ms). Scale bar: 2 µm. Integration time: 2 ms per pixel. (B, C) Two exemplary antenna-based images of the same sample (with 181 counts/ms and 26 counts/ms in acceptor and donor channels respectively). Scale bar: 500 nm. Integration time: 10 ms per pixel. Insets in A and B show lines profiles on two different fluorescence spots illustrating the increased lateral resolution obtained by the antenna (B) as compared to diffraction-limited confocal image (A). (D) *Upper plot:* E_{FRET} histogram obtained from the mean intensity of individual spots from multiple confocal images (blue) together with simulated data considering all possible orientations between donors and acceptors (grey). *Lower plot:* Corresponding E_{FRET} histogram obtained from individual spots over multiple antenna-based images.

images should mainly correspond to out-of-plane oriented molecules, which are expected given the larger field enhancement in the z direction.

The FRET efficiency can be experimentally determined as $E_{FRET} = \frac{n_a}{n_a + n_d}$, where n_a corresponds the number of photons collected in the acceptor channel (after background subtraction), and n_d to the photons collected in the donor channel (background subtracted and after applying a correction factor that accounts for the difference in fluorescence collection efficiencies between both channels, see Section 4). Figure 3D shows the histograms of E_{FRET} obtained from the mean intensities of individual spots over multiple confocal images (*upper plot*). The distribution is strongly shifted towards high FRET efficiencies around 90%. It is worth noticing that in our case the FRET pairs are immobilized and thus the relative orientation between the acceptor and the donor is fixed, as opposed to most FRET experiments performed in solution where the dyes are freely rotating. In this latter case the orientational factor κ^2 should be considered 2/3, obtained from averaging all orientations, whereas in our case all possible κ values ranging from 0 to one should exist. To assess the effect of κ on the experimentally determined E_{FRET} from confocal images, we generated a histogram from simulated data considering random orientations between the donor and the acceptor. Both experimental and simulated histograms agree nicely with each other validating our experimental approach and detection efficiencies in both channels (Figure 3D, *upper plot*).

Figure 3D (*lower plot*) shows the E_{FRET} distribution obtained from multiple antenna-based images. For this calculation, we consider the mean intensity of each individual spot, i.e. monopole excitation, disregarding the shadow contribution from the BNA arms. Both confocal and antenna-based E_{FRET} plots are quite similar with a mean E_{FRET} of 0.86 (sd = 0.20) and 0.88 (sd = 0.14) for confocal and antenna excitations respectively. While averaging over all antenna-FRET sample positions and orientations, the initial analysis shows therefore no significant effect of the antenna on the 3.4 nm average FRET efficiency distribution.

To gain further insight on the potential effect of the antenna position with respect to the FRET pairs, we reanalyse each fluorescence spot and generate E_{FRET} maps on a pixel-to-pixel level. Representative fluorescence and corresponding E_{FRET} maps with a 8 nm lateral resolution (corresponding to the pixel size) are shown in Figure 4A, B, respectively, together with exemplary zoom-in FRET spots (Figure 4C). Interestingly, the FRET efficiency is not homogenous or constant for each single pair, but instead it shows variations up to ~ 20% as a function of the antenna position with respect to individual FRET pairs. Moreover, distinct spatial patterns are observed for different pairs. These effects are more clearly visible when increasing the pixel resolution to 2 nm (Figure 4D, E) and unequivocally demonstrate nanoscale FRET modulation as a function of the antenna position.

To quantify better these FRET variations, we generate normalized donor and acceptor fluorescence line profiles on several FRET spots, obtained with a

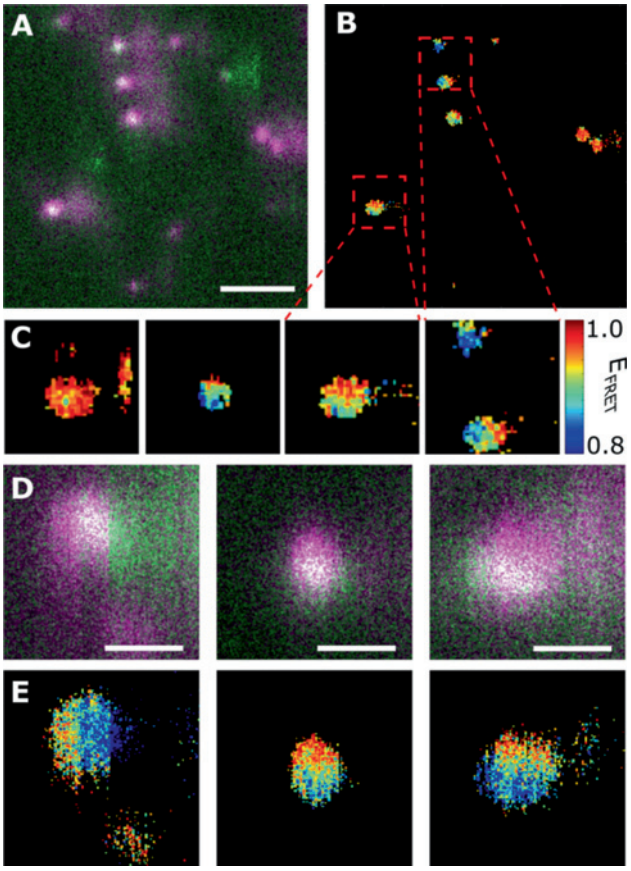

Figure 4: (A) Representative antenna-based image of individual FRET pairs after renormalizing the signal in the donor channel to its maximum. The sample is line-scanned along the vertical direction. Scale bar: 500 nm. (B) Corresponding E_{FRET} map calculated on a pixel-by-pixel basis after applying a 2×2 pixel Gaussian filter to the original image for better visualization. (C) Zoom-ins of different E_{FRET} spots with a lateral resolution of 8 nm (pixel size). Each spot shows a different spatial E_{FRET} pattern and pixel-to-pixel variations of E_{FRET} are readily observed. (D, E) Individual intensity and E_{FRET} spots respectively, mapped with a lateral resolution of 2 nm (corresponding to the pixel size). Notice that on the left panel photobleaching of the acceptor occurs during scanning so that the donor signal (green) is recovered and FRET is lost, further demonstrating that our measurements are performed at the level of single FRET-pairs. Scale bars: 200 nm. Integration time: 10 ms per pixel.

pixel resolution of 8 nm (Figure 5). To exclude the influence of residual excitation from the BNA arms, the line profiles are generated vertically along the *y*-scanning direction. Moreover, to reduce the effect of photon statistical fluctuations and any other photodynamic effects (such as blinking or flickering), we averaged over three line profiles. We assign the zero position in the *x*-axis to the pixel where donor signal is maximal. We further perform a Gaussian fitting of the line profiles from the two channels, and from there we calculate E_{FRET} as a function of the antenna position (black lines in Figure 5, and expanded on the upper plots) for those pixels where the signal from either of the two channels is at least 20% of its maximum. As observed from the different pairs, the FRET efficiency is not constant but it rather shows variations as a function of the lateral distance between the antenna and the FRET pair. The degree of FRET modulation ranges from 3% up to 15%, depending on the FRET pair. Furthermore, each FRET profile exhibits a different pattern: in most cases, the largest FRET reduction occurs close to centre (i.e. $x = 0$), while in some cases, a gradient from lower to higher FRET values is obtained. This effect is observed on those pairs where the spots in acceptor and green channels are laterally displaced with respect to each other, and occurs because of a different coupling of the antenna to the donor and acceptor, which in turn depends on the dipole orientation of the donor/acceptor with respect to the antenna and the respective donor and acceptor dipolar orientations. Overall, these results show nanoscale FRET modulation mapped with a spatial resolution of ~8 nm and at the single FRET pair level.

To understand the influence of the antenna position on the degree of FRET modulation, we performed FDTD simulations. The FRET efficiency is defined as a function of both the FRET and total donor rates (k_{FRET}, k_d). By rewriting equation 1, we can express E_{FRET} as a function of quantities that can be readily simulated:

$$E_{FRET}(r) = \frac{\frac{k_{FRET}(r)}{k^0_{FRET}}}{\frac{k_{FRET}(r)}{k^0_{FRET}} + \frac{k_d(r)}{k^0_{FRET}}} = \frac{\frac{k_{FRET}(r)}{k^0_{FRET}}}{\frac{k_{FRET}(r)}{k^0_{FRET}} + \frac{k_d(r)}{k^0_d}\frac{k^0_d}{k^0_{FRET}}} \tag{2}$$

where $\frac{k_{FRET}(r)}{k^0_{FRET}}$ is the FRET rate enhancement, that can be computed as the ratio of the field emitted by the donor at the acceptor position in presence and absence of the antenna [28], and $\frac{k_d(r)}{k^0_d}$ is the change in the total decay donor rates in presence and absence of the antenna. Finally, $\frac{k^0_d}{k^0_{FRET}}$ can be retrieved from the value of the FRET efficiency in a homogeneous environment

$$E^0_{FRET} = \frac{k^0_{FRET}}{k^0_{FRET} + k^0_d} = \frac{1}{1 + \frac{k^0_d}{k^0_{FRET}}} = \frac{1}{1 + \left(\frac{R}{R_0}\right)^6} \rightarrow \frac{k^0_d}{k^0_{FRET}} = \left(\frac{R}{R_0}\right)^6 \tag{3}$$

Therefore, the FRET efficiency at each antenna position is the result of a competition between the antenna induced FRET rate enhancement and donor rate enhancement [36, 37]. Overall, the condition for enhancement of the FRET efficiency [36] requires that $\frac{k_{FRET}(r)}{k^0_{FRET}} > \frac{k_d(r)}{k^0_d}$. Since both parameters depend on the relative position of the donor with respect to the antenna, we expect a modulation of the FRET efficiency while scanning the antenna over the FRET pairs.

Figure 6 shows the results of the FDTD simulations, considering two different axial distances from the antenna to the FRET pairs, i.e. $z = 10$ nm (Figure 6A) and $z = 30$ nm (Figure 6B). Simulations are performed for all three possible orientations of both the donor and acceptor, and for an antenna that scans the donor in the *y* direction, similar to our experimental settings. Moreover, we particularly focus on the influence of the antenna on the donor field as it is the one mostly affecting the acceptor.

As observed from the simulations considering FRET pairs with a short separation of 3.4 nm between donor and acceptor emitters, the donor rate enhancement $\frac{k_d(r)}{k^0_d}$, is always much higher than the FRET rate enhancement $\frac{k_{FRET}(r)}{k^0_{FRET}}$, for any donor orientation. Therefore, as the ratio $\frac{k^0_d}{k^0_{FRET}}$ is a constant for this FRET sample, the variations observed on the FRET efficiency directly represent the modulation of the donor LDOS as a function of the antenna position. Furthermore, since $\frac{k_d(r)}{k^0_d}$ is independent on the acceptor orientation, the FRET efficiency modulation by the antenna only depends on the donor orientation. Moreover, the strength of the FRET efficiency modulation depends on the dipolar orientation of the donor, being more pronounced for *z*-oriented donors as they couple more efficiently with the antenna (third row on Figure 6A, B). Since the near-field excitation provided by the antenna is stronger in the *z* direction (Figure 2), donors aligned along the *z* direction will be most efficiently excited and FRET will largely proceed from these pairs. In these conditions, we expect from our simulations to preferentially measure a FRET efficiency reduction, as transfer to the antenna competes with FRET transfer to the acceptor, which is fully consistent with our experimental results. Finally, the strength of FRET modulation strongly depends on the axial distance separation between the antenna and the donor emitter (simulations at $z = 10$ nm in Figure 6A and $z = 30$ nm for Figure 6B). At

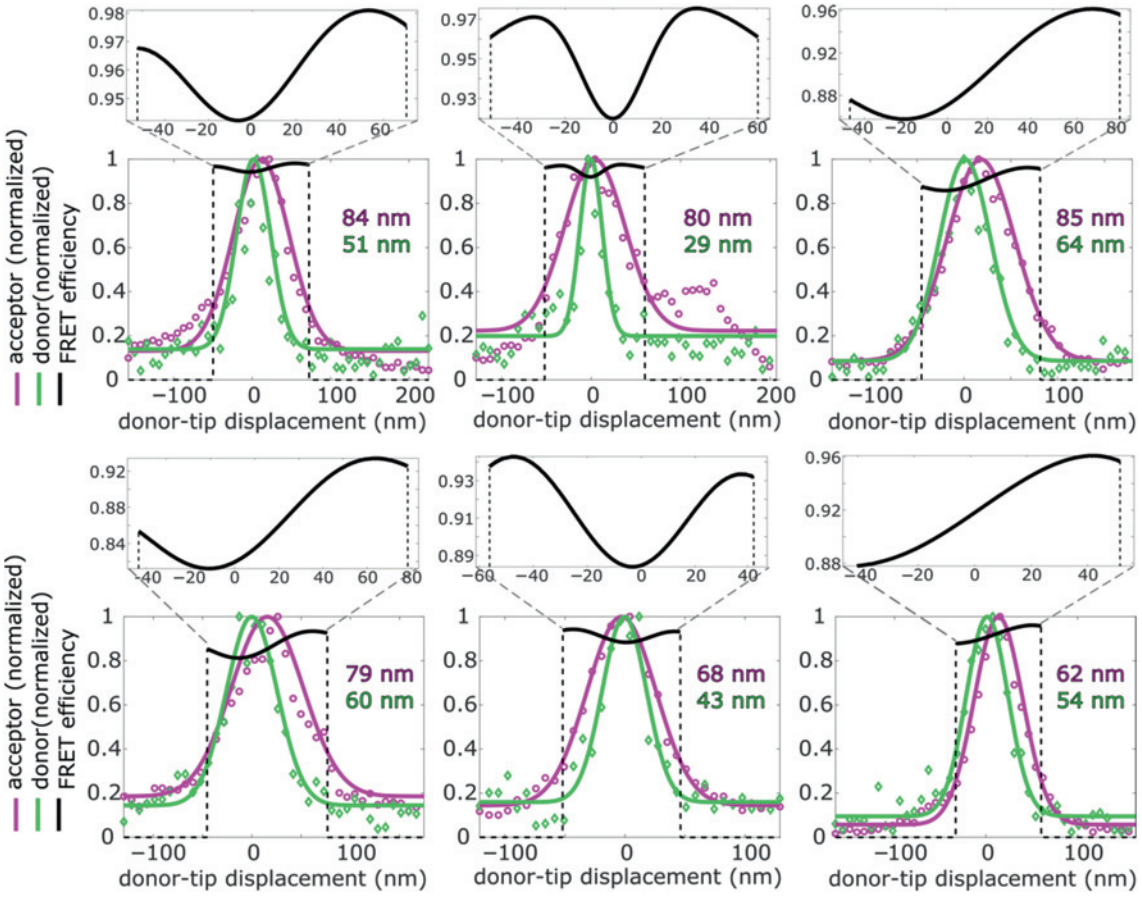

Figure 5: Line profiles of several FRET spots as a function of the antenna position taken along the *y*-scanning direction. Magenta represents the normalized signal from the acceptor channel, green from the donor channel and black corresponds to the FRET efficiency. Top insets are expanded plots of the FRET efficiency lines profiles. The zero position in the *x*-axis is defined at the pixel where the donor signal is maximum. The numbers on the right of each profile correspond to the respective FWHMs of donor and acceptor, obtained from Gaussian fittings to the experimental data.

z = 10 nm the drop in FRET efficiency caused by the donor enhancement rate is 40% and decreases to ~10% for an axial separation of 30 nm. Bearing in mind our sample preparation procedure where the FRET pairs are buried within a thin 10 nm PMMA layer, and that the distance between the antenna and the sample in NSOM experiments is between 5 and 10 nm given by the feedback loop, we estimate an axial separation of 15–20 nm between the antenna and the FRET pairs. Thus, our experimentally obtained FRET modulation values of 3–13% agree well with an axial distance separation between the antenna and the donor that lies between the two simulated sets (Figure 6A, B).

Interestingly, the experimental data shown in Figure 5 also shows a consistent narrower profile of the donor signal as compared to the acceptor one. To enquire whether this observation is statistically significantly, we analysed over 30 different FRET spots and measured their FWHM (Figure 7A). The histogram shows a clear narrowing of the FWHM distributions of the donor compared to the acceptor profiles, with as much as ~ 30 nm. To exclude any potential artefacts induced by the antenna and/or the experimental set-up we performed similar measurements on 20 nm-beads (labelled with nile red) deposited on glass coverslips (Figure 7B). As expected, the FWHM distributions for both channels fully overlap with each other, indicating that the FWHM shift between donor and emission profiles should arise from the coupling of the antenna to the FRET pairs. Notice that we assign a narrowing of the donor profile rather than a broadening of the acceptor FWHM, since the FRET pairs are buried in the PMMA layer and thus at a larger z

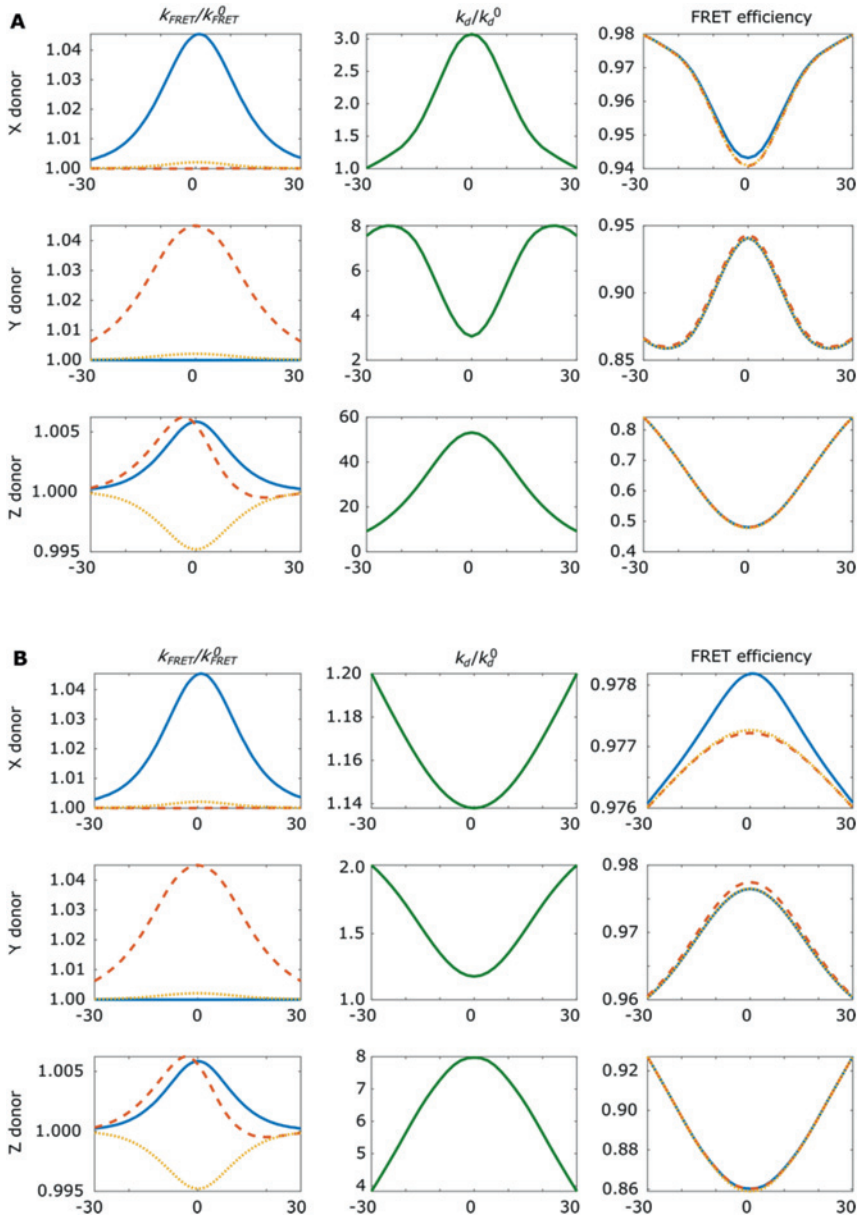

Figure 6: (A, B) FDTD simulations of FRET rate enhancement (left column), donor rate enhancement (middle column) and resulting FRET efficiency (right column) as a function of the lateral antenna position with respect to the donor. The simulations are performed assuming that the acceptor is parallel to the donor and positioned 3.4 nm away from the donor. The *x*-axes on the plots correspond to the lateral distance (in nanometres) of the antenna with respect to the donor, i.e. as the antenna scans the donor in the *y* direction in analogy to the experimentally obtained line profiles. $x = 0$ corresponds to the position where the antenna is vertically aligned with the donor. Simulations are shown for different dipolar orientations of the donor (*x* in first row, *y* in the second and *z* in the third row) and consider the 3D near-field components emitted by the donor (in the *x*-direction: solid blue, in the *y*-direction: dashed red and in the *z*-direction: dotted yellow). In the case of the donor rate enhancement, only the donor orientation plays a role (shown as green lines). The simulations are shown for an axial separation between the donor and the monopole end of (A) 10 nm and (B) 30 nm.

distance, as compared to the beads which are much closer to the antenna. Therefore, the FWHM acceptor broadening is simply the result of its axial separation with respect to the antenna. In strong contrast, the narrowing of the donor profile occurs as a result of FRET and donor coupling to the antenna. These results can be understood on the basis that E_{FRET} results from a competition between enhanced k_d and k_{FRET} (Figure 7C). Based on our simulations (Figure 6), at lateral positions away from the antenna, k_{FRET} dominates and the donor signal is highly quenched. However, at lateral positions close to the antenna (within ~ ± 15 nm as inferred from Figure 6), the donor rate enhancement is highly increased and competes with k_{FRET}, leading to donor emission unquenching. Our experimental data agrees remarkably well with the simulations, as the donor FWHM profile is ~ 30 nm narrower than the acceptor emission profile. In summary, by laterally manipulating with nanometric precision the 3D position of the antenna with respect to the emitters, we are able to directly map the competition between k_d and k_{FRET} and experimentally measure FRET modulation induced by photonic antennas.

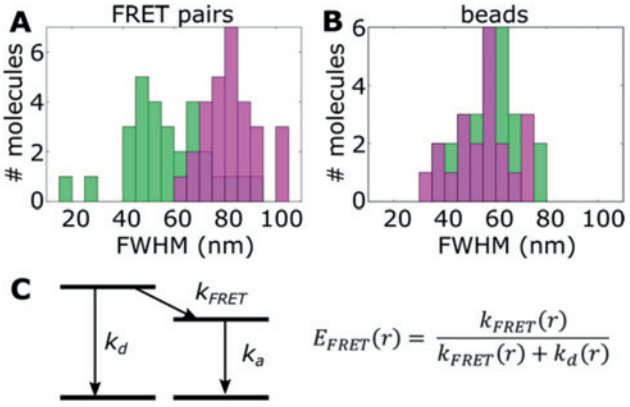

Figure 7: (A) Histogram of the FWHM obtained from different FRET pairs, where green and magenta correspond to donor and acceptor emitters, respectively. (B) Corresponding histogram obtained on 20 nm beads measured using the same antenna and under similar experimental conditions. (C) Schematics of the FRET process, where k_a (acceptor emission rate) depends on the competition between k_d and k_{FRET}.

3 Conclusions

In this work we have used nanoantennas mounted on a near-field optical set-up to achieve full 3D control of the antenna position with respect to single FRET pairs. Using this approach, we have directly mapped the FRET efficiency as a function of the antenna-pair distance, with an unprecedented lateral control of 2 nm. Our experiments confirm that the resulting energy transfer depends on the position of the antenna with respect to the pair and on the donor dipole orientation, in agreement with previous works [19, 26]. For a system with high FRET efficiency such as the one studied here (3.4 nm separation), the donor enhancement rate dominates over the FRET rate resulting in an overall decrease of FRET efficiency between 3 and 15%. Our work constitutes the first experimental spatial mapping of the influence of photonic antennas on the competition between k_d and k_{FRET}, controlling the FRET efficiency. It will be interesting to study in the future similar effects on FRET pairs of larger separations [19, 26]. Such experiments will be interesting given the broad applicability of FRET and the prospect that photonic antennas can extend the range at which FRET can be observed.

4 Materials and methods

Tip fabrication: The hybrid antennas were carved by FIB (Zeiss Auriga 60 FIB-SEM, 1 nm resolution GEMINI scanning electron microscope (SEM), equipped with Orsay Optics 2.5 nm-resolution Cobra ion column) at the end face of aluminium-coated tapered optical fibres. The tapers were created by heating & pulling single mode (SM600, Fibercore) optical fibres. A 150 nm aluminium layer was deposited by thermal evaporation (Oerlikon Leybold Univex 350) around the fibres to prevent light leakage from the tapered region. The apex of the coated probes was then removed by FIB to create a well-defined glass opening with diameters close to the cut-off region (500–600 nm) such as to sustain the lowest order mode (TM01). The milled end faces were then coated with a 200 nm thick aluminium layer. Monopole antennas (60 to 80 nm long, 30 to 50 nm wide) were first carved into the layer, and BNAs were then milled into the remaining metal in close proximity to the monopole (with dimensions 300 × 300 nm and a reproducible gap of 30 nm).

FRET pairs preparation: Double-stranded DNA constructs of 51 base pairs length were designed with one Atto550 donor on the forward strand, and one Atto647N acceptor on the reverse strand [19]. The distance between fluorescent labels was set such that the donor and acceptor are separated by 10 base pairs (corresponding to 3.4 nm separation). As 10 base pairs make a complete turn on the DNA double strand, the choice of D–A separation as a multiple of 10 base pairs avoids considering the complex three-dimensional structure of DNA to estimate the D–A distance. The characteristic Förster radius computed for atto550 and atto647N in pure water is 6.5 nm. Labelled HPLC-purified DNA single strands are obtained from IBA (Göttingen, Germany), modified with the corresponding *N*-hydroxysuccinimidyl ester (NHS) donor and acceptor fluorophore derivatives of atto550 and atoo647N. Fluorophores were covalently linked to an amino-C6-modified thymidine with NHS-chemistry via base labelling. The forward strand sequence is 5′-CCTGAGCGTACTGCAGGATAGCCTATCGCGTGTCA-TATGCTGTT$_D$CAGTGCG-3′. The reverse strand sequence is 5′-CGCACT-GAACAGCATAT$_A$GACACGCGATAGGC TATCCTGCAGTACGCTCAGG-3′. The subscripts indicate the bases where the fluorophores are being attached (A for the acceptor and D for the donor). The strands were annealed at 10 µM concentrations in 40 mM Tris-Acetate, 1 mM EDTA, 12.5 mM $MgCl_2$ buffer, and by heating to 95 °C for 5 min followed by slow cooling to room temperature. The double stranded DNA stocks were diluted in a 10 mM HEPES buffer, pH 7, and stored at –20 °C.

Sample preparation: Glass coverslips where coated with a thin (~10 nm) layer of PMMA by spin coating at 6000 rpm. Afterwards, FRET pairs were diluted in HEPES to a concentration of 10 nM and spin coated onto these PMMA-coated coverslips at 2000 rpm. This ensures that single pairs will be well separated for imaging and that the FRET pairs will lie on top of the PMMA layer. Finally, a second thin layer of PMMA (~ 10 nm) was spin coated (6000 rpm) on top to improve immobilization of the FRET pairs and increase the photostability of the dyes.

Numerical simulations: 3D numerical modelling on hybrid antenna probes was based on the finite-difference time-domain (FDTD) simulations. For the simulations on the field enhancement, the model considers a volume spanning 5 µm in *x*, *y* and 8.5 µm in *z*. The refraction index and taper angle of the dielectric body of the probe were chosen to be 1.448 and 24°, respectively. The aluminium thickness on the side and on the end face of the tips is 150 and 120 nm, respectively, and the aluminium dielectric constant was measured by ellipsometry. The external dimensions of the BNA are 300 nm, and the gap size is 30 nm. The monopole antenna length and diameter are chosen to be 70 and 30 nm, respectively. A nonuniform grid resolution varies from 25 nm for portions at the periphery of the simulation, 5 nm for the region in the immediate proximity to the BNA, and to 1 nm for the volume including the monopole antenna. Excitation at λ = 561 nm was done by a linearly polarized Gaussian beam launched at 7 µm away from the tip body

and propagating toward the hybrid antenna. The field profiles are measured at a *xy*-plane 10 nm away from the monopole end.

For the simulations of the rate enhancements the antennas are simulated on a glass substrate positioned in the middle of a FDTD window spanning ±1 µm in *x*, *y* and *z*, in order to reduce the running time. In addition, to be closer to the experimental conditions (FWHM from beads ~55 nm), we chose a monopole diameter of 50 nm. The rest of the parameters are kept the same as mentioned before.

FRET efficiency calculation: For every pixel in the spots observed we record the number of photons in both acceptor and donor channels (n_a and n_d, respectively). The background on each channel is then subtracted from these values. The FRET efficiency is then computed on every pixel according to the formula $E_{FRET} = \frac{n_a}{n_a + \gamma n_d}$, where γ accounts for the different detection efficiencies of donor and acceptor channels for every optical element in the optical detection path. Considering the fluorescence collection efficiencies of the objective and the APDs at the emission maxima of the donor and the acceptor, together with the transmission of all of the filters in use (dichroic and band passes used to split and filter the collected fluorescence signal) in the emission range of both donor and acceptor dyes, we estimate this correction factor to be $\gamma = 0.76$. Here, we assume that this factor is mostly unaffected by the antenna. This hypothesis is confirmed by the good agreement between the experiments and the FDTD simulations.

Acknowledgements: The authors would like to thank F. Campelo for simulations of FRET efficiencies in the confocal configuration and useful discussions. The research leading to these results has received funding from the European Commission H2020 Program under grant agreement ERC Adv788546 (NANO-MEMEC), the Spanish Ministry of Economy and Competitiveness ("Severo Ochoa" Programme for Centres of Excellence in R&D (SEV-2015-0522), FIS2015-63550-R, FIS2017-89560-R and BES-2015-072189), Fundació CELLEX (Barcelona), CERCA Programme/Generalitat de Catalunya Fundació Mir-Puig and the Agence Nationale de la Recherche (ANR) under grant agreement ANR-17-CE09-0026-01.

Author contribution: All the authors have accepted responsibility for the entire content of this submitted manuscript and approved submission.

Research funding: None declared.

Conflict of interest statement: The authors declare no conflicts of interest regarding this article.

References

[1] L. Novotny and N. F. van Hulst, "Antennas for light," *Nat. Photon*, vol. 5, no. 83, 2011, https://www.nature.com/articles/nphoton.2010.237.

[2] T. S. Van Zanten, J. Gómez, C. Manzo, et al., "Direct mapping of nanoscale compositional connectivity on intact cell membranes," *PNAS*, vol. 107, no. 35, p. 15437, 2010.

[3] A. Puchkova, C. Vietz, E. Pibiri, et al., "DNA Origami Nanoantennas with over 5000-fold fluorescence enhancement and single-molecule detection at 25 µM," *Nano Lett.*, vol. 15, no. 12, p. 8354, 2015.

[4] P. M. Winkler, R. Regmi, V. Flauraud, et al., "Antenna-based fluorescence correlation spectroscopy to probe the nanoscale dynamics of biological membranes," *J. Phys. Chem. Lett.*, vol. 9, no. 1, p. 110, 2018.

[5] J. Wenger, D. Gérard, J. Dintinger, et al., "Emission and excitation contributions to enhanced single molecule fluorescence by gold nanometric apertures," *Opt. Express*, vol. 16, no. 5, p. 3008, 2008.

[6] P. Anger, P. Bharadwaj, and L. Novotny, "Enhancement and quenching of single-molecule fluorescence," *Phys. Rev. Lett.*, vol. 96, p. 113002, 2006.

[7] P. Bharadwaj, P. Anger, and L. Novotny, "Nanoplasmonic enhancement of single-molecule fluorescence," *Nanotechnology*, vol. 18, p. 044017, 2007.

[8] A. Kinkhabwala, Z. Yu, S. Fan, Y. Avlasevich, K. Müllen, and W. E. Moerner, "Large single-molecule fluorescence enhancements produced by a bowtie nanoantenna," *Nat. Photon.*, vol. 3, no. 11, p. 654, 2009.

[9] D. Punj, M. Mivelle, S. B. Moparthi, et al., "A plasmonic 'antenna-in-box' platform for enhanced single-molecule analysis at micromolar concentrations," *Nat. Nanotechnol.*, vol. 8, no. 7, p. 512, 2013.

[10] V. Flauraud, R. Regmi, P. M. Winkler, et al., "In-plane plasmonic antenna arrays with surfacenanogaps for giant fluorescence enhancement," *Nano Lett.*, vol. 17, no. 3, p. 1703, 2017.

[11] M. Mivelle, T. S. Van Zanten, and M. F. Garcia-Parajo, "Hybrid photonic antennas for subnanometer multicolor localization and nanoimaging of single molecules," *Nano Lett.*, vol. 14, no. 8, p. 4895, 2014.

[12] K. A. Willets, A. J. Wilson, V. Sundaresan, and P. B. Joshi, "Super-resolution imaging and plasmonics," *Chem. Rev.*, vol. 117, no. 11, p. 7538, 2017.

[13] K. Truong and I. Mitsuhiko, "The use of FRET imaging microscopy to detect protein-protein interactions and protein conformational changes in vivo," *Curr. Opin. Struct. Biol.*, vol. 11, no. 5, p. 573, 2001.

[14] R. Rahul, S. Hohng, and T. Ha, "A practical guide to single molecule FRET," *Nat. Methods*, vol. 5, p. 507, 2008.

[15] P. Andrew and W. L. Barnes, "Forster energy transfer in an optical microcavity," *Science*, vol. 290, no. 5492, p. 785, 2000. (80-).

[16] R. M. Clegg, "Fluorescence resonance energy transfer," *Curr. Opin. Biotechnol.*, vol. 6, p. 103, 1995.

[17] E. Lerner, T. Cordes, A. Ingargiola, et al., "Toward dynamic structural biology: two decades of single-molecule Förster resonance energy transfer," *Science*, vol. 359, p. 6373, 2018.

[18] J. de Torres, M. Mivelle, S. B. Moparthi, et al., "Plasmonic nanoantennas enable forbidden Förster dipole-dipole energy transfer and enhance the FRET efficiency," *Nano Lett.*, vol. 16, no. 10, p. 6222, 2016.

[19] P. Ghenuche, M. Mivelle, J. De Torres, et al., "Matching nanoantenna field confinement to FRET distances enhances Förster energy transfer rates," *Nano Lett.*, vol. 15, no. 9, p. 6193, 2015.

[20] N. Aissaoui, K. Moth-Poulsen, M. Käll, P. Johansson, L. M. Wilhelmsson, and B. Albinsson, "FRET enhancement close to

gold nanoparticles positioned in DNA origami constructs," *Nanoscale*, vol. 9, p. 673, 2017.

[21] C. Blum, N. Zijlstra, A. Lagendijk, et al., "Nanophotonic control of the Förster resonance energy transfer efficiency," *Phys. Rev. Lett.*, vol. 109, p. 203601, 2012.

[22] A. Konrad, M. Metzger, A. M. Kern, M. Brecht, and A. J. Meixner, "Controlling the dynamics of Förster resonance energy transfer inside a tunable sub-wavelength Fabry-Pérot-resonator," *Nanoscale*, vol. 7, no. 22, p. 10204, 2015.

[23] K. Rustomji, M. Dubois, B. Kuhlmey, et al., "Direct imaging of the energy-transfer enhancement between two dipoles in a photonic cavity," *Phys. Rev. X*, vol. 9, p. 011041, 2019.

[24] J. R. Zurita-Sánchez and J. Méndez-Villanueva, "Förster Energy transfer in the vicinity of two metallic nanospheres (Dimer)," *Plasmonics*, vol. 13, no. 3, p. 873, 2018.

[25] P. Ghenuche, J. De Torres, S. B. Moparthi, V. Grigoriev, and J. Wenger, "Nanophotonic enhancement of the Förster resonance energy-transfer rate with single nanoapertures," *Nano Lett.*, vol. 14, no. 8, p. 4707, 2014.

[26] M. Baibakov, S. Patra, J.-B. Claude, A. Moreau, J. Lumeau, and J. Wenger, "Extending single-molecule Förster resonance energy transfer (FRET) Range beyond 10 nanometers in zero-mode waveguides," *ACS Nano*, vol. 13, no. 7, p. 8469, 2019.

[27] J. Zhang, Y. Fu, M. H. Chowdhury, and J. R. Lakowicz, "Enhanced Förster resonance energy transfer (FRET) on a single metal particle," *J. Chem. Phys.*, vol. 111, no. 1, p. 50, 2007.

[28] B. Schreiber, M. Kauk, H. S. Heil, et al., "Enhanced fluorescence resonance energy transfer in G-Protein-coupled receptor probes on nanocoated microscopy coverslips," *ACS Photon.*, vol. 5, no. 6, p. 2225, 2018.

[29] T. Zhao, T. Li, and Y. Liu, "Silver nanoparticle plasmonic enhanced förster resonance energy transfer (FRET) imaging of protein-specific sialylation on the cell surface," *Nanoscale*, vol. 9, p. 9841, 2017.

[30] A. G. Curto, G. Volpe, T. H. Taminiau, M. P. Kreuzer, R. Quidant, and N. F. van Hulst, "Unidirectional emission of a quantum dot coupled to a nanoantenna," *Science*, vol. 329, no. 5994, p. 930, 2010. (80-).

[31] T. H. Taminiau, F. D. Stefani, and N. F. Van Hulst, "Single emitters coupled to plasmonic nano-antennas: angular emission and collection efficiency," *New J. Phys.*, vol. 10, no. 10, p. 105005, 2008.

[32] K. Yao and Y. Liu, "Controlling electric and magnetic resonances for ultracompact nanoantennas with tunable directionality," *ACS Photon.*, vol. 3, no. 6, p. 953, 2016.

[33] K. Hübner, M. Pilo-Pais, F. Selbach, et al., "Directing single-molecule emission with DNA Origami-assembled optical antennas," *Nano Lett.*, vol. 19, no. 9, p. 6629, 2019.

[34] L. Novotny and B. Hecht, *Principle of Nano-Optics*, Cambridge, Cambridge University Press, 2006.

[35] J. Bohlen, A. Cuartero-González, E. Pibiri, et al., "Plasmon-assisted Förster resonance energy transfer at the single-molecule level in the moderate quenching regime," *Nanoscale*, vol. 11, no. 16, p. 7674, 2019.

[36] C. L. Cortes and Z. Jacob, "Fundamental figures of merit for engineering Förster resonance energy transfer," *Opt. Express*, vol. 26, no. 15, p. 19371, 2018.

[37] S. Bidault, A. Devilez, P. Ghenuche, B. Stout, N. Bonod, and J. Wenger, "Competition between Förster resonance energy transfer and donor photodynamics in plasmonic dimer nanoantennas," *ACS Photon*, vol. 3, p. 895, 2016.